

---

# OrderFusion: Encoding Orderbook for Probabilistic Intraday Price Prediction

---

Runyao Yu<sup>1,2</sup> Yuchen Tao<sup>3</sup> Fabian Leimgruber<sup>2</sup> Tara Esterl<sup>2</sup> Jochen L. Cremer<sup>1,2</sup>

## Abstract

Efficient and reliable probabilistic prediction of intraday electricity prices is essential to manage market uncertainties and support robust trading strategies. However, current methods often suffer from parameter inefficiencies, as they fail to fully exploit the potential of modeling interdependencies between bids and offers in the orderbook, requiring a large number of parameters for representation learning. Furthermore, these methods face the *quantile crossing* issue, where upper quantiles fall below the lower quantiles, resulting in unreliable probabilistic predictions. To address these two challenges, we propose an encoding method called *OrderFusion* and design a hierarchical multi-quantile head. The OrderFusion encodes the orderbook into a 2.5D representation, which is processed by a tailored jump cross-attention backbone to capture the interdependencies of bids and offers, enabling parameter-efficient learning. The head sets the median quantile as an anchor and predicts multiple quantiles hierarchically, ensuring reliability by enforcing monotonicity between quantiles through non-negative functions. Extensive experiments and ablation studies are conducted on four price indices: 60-min ID<sub>3</sub>, 60-min ID<sub>1</sub>, 15-min ID<sub>3</sub>, and 15-min ID<sub>1</sub> using the German orderbook over three years to ensure a fair evaluation. The results confirm that our design choices improve overall performance, offering a parameter-efficient and reliable solution for probabilistic intraday price prediction.

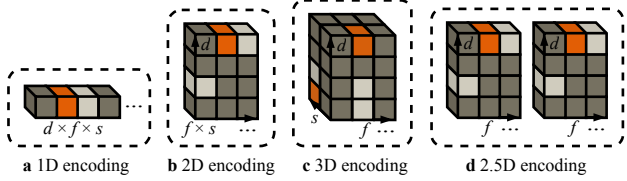


Figure 1. Comparison of encoding methods for orderbook. **a**, Orderbook data are flattened into a 1D vector with a dimension of  $(d \times f \times s)$ , where  $d$ ,  $f$ ,  $s$  denote for the number of look-back window lengths (explained in Section 4.1), number of features, and number of sides (bid and offer), respectively. **b**, Orderbook data are reshaped into a 2D time-series form with a dimension of  $(d, f \times s)$ . **c**, Orderbook data are organized into a 3D pseudo image form with a dimension of  $(d, f, s)$ . **d**, Orderbook data are split into two 2D matrices, one for each side (bid or offer) with a dimension of  $(d, f)$ , to form a “2.5D” encoding (ours).

## 1. Introduction

The rapid expansion of wind and solar energy in recent years introduces significant variability in power generation due to weather dependence. This variability often leads to forecasting errors in wind and solar power output, resulting in power system imbalances with the energy demand (Koch & Hirth, 2019).

The continuous intraday (CID) market plays a pivotal role in addressing this imbalance challenge. The CID market opens at 15:00 the previous day, allowing participants to adjust for unplanned energy imbalances arising from forecast errors in wind and solar power generation, up to five minutes before electricity delivery (Narajewski & Ziel, 2020b). As a result, the CID market significantly alleviates the demands on balancing energy (Ocker & Ehrhart, 2017). With the growing adoption of algorithmic trading in the CID market, intraday price prediction is crucial to managing uncertainties and optimizing trading strategies (Hirsch & Ziel, 2024b).

The CID market operates under *weak-form efficiency*. This concept states that recent market prices reflect past publicly available trading information. Various studies (Monteiro et al., 2016; Andrade et al., 2017; Janke & Steinke, 2019; Uniejewski et al., 2019; Narajewski & Ziel, 2020a;b; Hirsch & Ziel, 2024b) found that while intraday prices are influenced by factors such as wind and solar energy generation,

---

<sup>1</sup>Department of Electrical Sustainable Energy, Delft University of Technology, Delft, The Netherlands <sup>2</sup>Center for Energy, Austrian Institute of Technology, Vienna, Austria <sup>3</sup>Institute for Automotive Engineering, RWTH Aachen, Aachen, Germany. Correspondence to: Runyao Yu <runyao.yu@tudelft.nl>.

day-ahead forecasts of these factors provide limited predictive power, since the information these factors carry is already reflected in recent market prices. Consequently, the most powerful predictors of future intraday price are extracted from recent trades in the orderbook.

In the context of intraday price prediction, there has been a gradual transition from pointwise prediction to probabilistic prediction. Pointwise prediction models, such as those explored in (Monteiro et al., 2016; Oksuz & Ugurlu, 2019; Uniejewski et al., 2019; Marcjasz et al., 2020; Narajewski & Ziel, 2020a), estimate a single future price value, are challenged to quantify market uncertainties. To address this limitation, probabilistic prediction models (Andrade et al., 2017; Narajewski & Ziel, 2020b; Serafin et al., 2022; Cramer et al., 2023; Hirsch & Ziel, 2024a;b) estimate potential price intervals by predicting price quantiles, providing a more nuanced understanding of market uncertainties.

However, these probabilistic approaches face several challenges. First, they often rely on simplified input representations, such as flattened 1D vectors or 2D time-series formats, which fail to fully capture the bid-offer interdependencies. As a result, learning meaningful representations requires a large number of parameters, leading to parameter inefficiency. Second, these methods frequently encounter quantile crossing issues, where higher quantiles are predicted to be lower than lower quantiles, violating the fundamental properties of probabilistic forecasting (Chernozhukov et al., 2010). This inconsistency results in unreliable probabilistic predictions, posing a challenge for decision-making in energy trading.

This paper proposes an encoding method called OrderFusion and designs a hierarchical multi-quantile head. OrderFusion converts the orderbook into a 2.5D representation, shown in Figure 1. A tailored jump cross-attention backbone takes 2.5D encoding as an input to model interdependencies between bid and offer sides. The head sets the median quantile as an anchor, predicts multiple quantiles hierarchically with a shared representation, and ensures that upper quantiles remain higher than lower ones by incorporating monotonic constraints, overcoming quantile crossing issues. Furthermore, we conduct case studies and ablation studies on four price indices: 60-min  $ID_3$ , 60-min  $ID_1$ , 15-min  $ID_3$ , and 15-min  $ID_1$  over three years.

### 1.1. Contribution

- We propose OrderFusion, an encoding method that models interdependencies between bids and offers with a tailored jump cross-attention backbone, enabling parameter-efficient learning.
- We design a hierarchical multi-quantile head that sets the median quantile as an anchor and predicts multi-

ple quantiles hierarchically, overcoming the quantile crossing issue and mitigating error accumulation.

- We conduct experiments and ablation studies to demonstrate the parameter efficiency and reliability of the proposed methods on four price indices over three years.

### 1.2. Roadmap

The rest of the paper is organized as follows: Section 2 reviews related works. Section 3 describes orderbook and price indices. Section 4 details the proposed methods. Section 5 presents experiments and ablation studies on four price indices. Finally, Section 6 concludes the paper.

## 2. Related Work

### 2.1. Cross-Attention

Cross-attention has proven to be a powerful mechanism for capturing complex dependencies in sequential and structured data across various fields. In multivariate time series forecasting, it enables the fusion of temporal and static feature embeddings, as demonstrated in (Lim et al., 2021) and (Zhang & Yan, 2023), enhancing predictive performance by modeling intricate relationships between variables. In computer vision, (Chen et al., 2021) uses cross-attention to combine multi-scale image patch embeddings, improving classification accuracy. Similarly, in point cloud processing, (Afham et al., 2022) applies cross-attention between 2D and 3D representations to learn richer shape features in a self-supervised manner, while (Fei et al., 2023) utilizes cross-attention to integrate global and local information. Despite its success in various domains, cross-attention remains underexplored in intraday price prediction. Our proposed OrderFusion tailored with a jump cross-attention backbone aims to model the bid-offer interdependencies.

### 2.2. Multi-Quantile Prediction and Quantile Crossing

Multi-quantile prediction frameworks are becoming increasingly popular to capture uncertainties in price forecasts. The studies (Rodrigues & Pereira, 2020; Jawed & Schmidt-Thieme, 2022) aim to reduce the complexity of training by jointly predicting several quantiles from a shared representation. However, a well-known issue is quantile crossing, where upper quantiles occasionally yield lower values than lower quantiles. This inconsistency violates the fundamental property of cumulative distribution functions and can drastically reduce the reliability of interval forecasts (Chernozhukov et al., 2010). Previous works attempt to fix crossing errors via post-processing methods such as simply re-sorting quantiles (Maciejowska & Nowotarski, 2016; Serafin et al., 2019; 2022). Although straightforward, such solutions risk distorting the learned distribution by imposing an artificial correction step. (Park et al., 2022) introduces

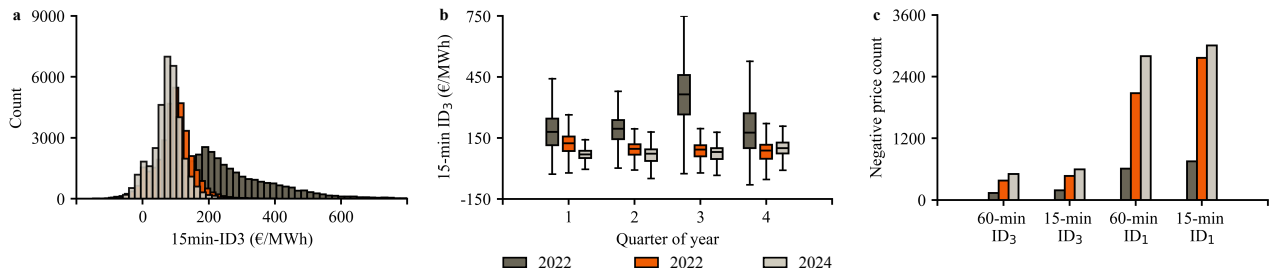


Figure 2. Distribution and seasonal patterns of four intraday price indices. **a**, The distribution of 15-min  $ID_3$  exhibits a noticeable shift from 2022 to 2023 and 2024, indicating increasing price stability within the normal range. **b**, The boxplot reveals a seasonal pattern of 15-min  $ID_3$  each year, with price fluctuations varying by quarter. **c**, The count of negative prices steadily rises over the years, reflecting the growing influence of renewable energy integration in the market.

---

### Algorithm 1 Orderbook Filtering

---

**Input:** Raw orderbook files  
 Initialize data structures for storing processed orders  
**for all** orderbook files **do**  
   Load orderbook  
   Classify orders by product type (hourly/quarter-hourly)  
   **if** hourly products exist **then**  
     Group records by OrderID and transaction time  
     Filter entries with action codes “P” or “M”  
     Compute traded volume between consecutive updates  
     Aggregate processed hourly trades  
   **end if**  
   **if** quarter-hourly products exist **then**  
     Apply the same processing steps as hourly products  
     Aggregate processed quarter-hourly trades  
   **end if**  
**end for**  
**Return** Aggregated and filtered orderbook

---

an incremental quantile function that anchors at the lowest quantile and employs non-negative functions, such as ReLU or Softplus, to learn positive residuals, which are then hierarchically added until reaching the highest quantile. However, this approach is prone to error accumulation through the process of iterative addition. Drawing inspiration from this design, we anchor at the median quantile and apply addition and subtraction to estimate tail quantiles, reducing the risk of error accumulation.

## 3. Data

### 3.1. Orderbook

The orderbook data purchased from the European Power Exchange Spot (EPEX Spot) provide detailed insights into electricity market dynamics. Specifically, the orderbook records trading activities with key attributes including *deliv-*

*ery start time of electricity, type of product, price, volume, side, OrderID, transaction time, and action code.*

The delivery start time of electricity marks the time at which electricity is physically delivered. Each distinct delivery start time corresponds to a unique *product*. For example, electricity deliveries starting at 08:00 and 09:00 are different products. In addition, there are several types of products, such as hourly (60-min) and quarter-hourly (15-min). Hourly products have delivery start times at standard hourly intervals, such as 10:00, 11:00, . . . , while quarter-hourly products start at finer intervals, such as 10:00, 10:15, . . . .

Up to five minutes before each delivery start time, traders can place orders, specifying price (€/MWh), volume (MWh), and side (bid or offer) with an OrderID assigned to the trader. If a bid or offer is matched, the transaction time is recorded and an action code is assigned: “M” (fully matched) or “P” (partially matched). A fully matched order means that the entire volume is traded, rendering the order inactive for future transactions. A partially matched order indicates that only a portion of the volume is executed, while the unexecuted volume remains in the system and can still be matched with other traders. The matching rule is introduced at a high level in Algorithm 2.

Furthermore, we filter out unmatched orders, as they do not contribute to market-clearing outcomes. The pseudocode of the filtering algorithm is described in Algorithm 1.

### 3.2. Price Indices

We focus on four popular price indices: 60-min  $ID_3$ , 60-min  $ID_1$ , 15-min  $ID_3$ , and 15-min  $ID_1$ . The 60-min and 15-min indices correspond to different product types, where electricity is delivered every 60 min and 15 min, respectively. The  $ID_3$  index represents the volume-weighted average price (VWAP) of all filtered trades executed within the last 3 trading hours before delivery, focusing on the most liquid period of a trading session. The  $ID_1$  index is calculated as

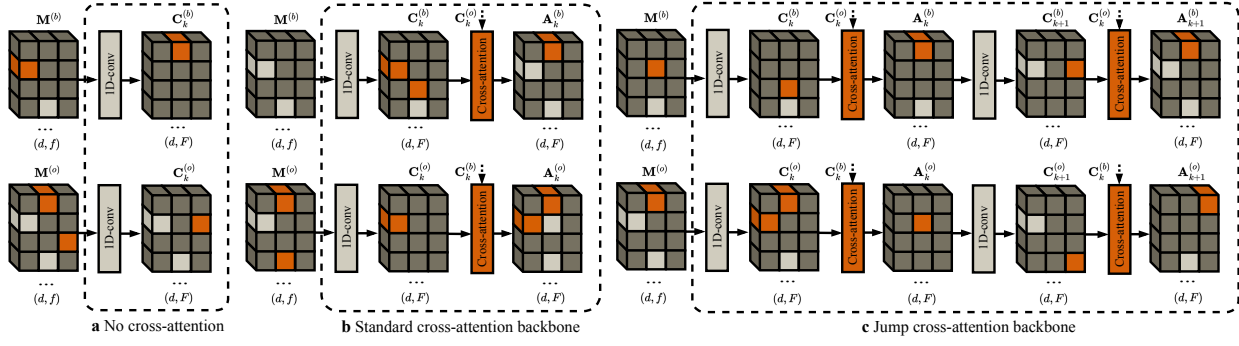


Figure 3. Comparison of different backbones. **a** No cross-attention. The inputs  $M^{(b)}$  and  $M^{(o)}$  independently pass through a 1D-conv layer, producing  $C_k^{(b)}$  and  $C_k^{(o)}$ , respectively. Each 1D-conv layer transforms the input shape to  $(d, f)$ . The outputs  $C_k^{(b)}$  and  $C_k^{(o)}$  then serve as inputs to the next block, generating  $C_{k+1}^{(b)}$  and  $C_{k+1}^{(o)}$ , and so on. **b** Standard cross-attention backbone. Initially follows the same process as block **a** to obtain  $C_k^{(b)}$  and  $C_k^{(o)}$ . Then,  $C_k^{(b)}$  serves as the query, and  $C_k^{(o)}$  as the key and value in a cross-attention layer to produce  $A_k^{(b)}$ . Then, the roles of query, key, and value are exchanged to generate  $A_k^{(o)}$ . This procedure is repeated for the next block to obtain  $A_{k+1}^{(b)}$  and  $A_{k+1}^{(o)}$ , and so on. **c** Jump cross-attention backbone. Initially follows the same process as block **b** to compute  $A_k^{(b)}$  and  $A_k^{(o)}$ . Then,  $A_k^{(b)}$  and  $A_k^{(o)}$  independently pass through a 1D-conv layer to obtain  $C_{k+1}^{(b)}$  and  $C_{k+1}^{(o)}$ , respectively. Unlike **b**, where  $A_{k+1}^{(b)}$  is obtained by processing  $C_{k+1}^{(b)}$  as the query and  $C_{k+1}^{(o)}$  as the key and value, the jump cross-attention block instead utilizes  $C_{k+1}^{(b)}$  as the query and  $C_{k+1}^{(o)}$  as the key and value to produce  $A_{k+1}^{(b)}$ . Similarly,  $A_{k+1}^{(o)}$  is obtained by exchanging the roles of query, key, and value. This procedure continues for subsequent blocks. The design encourages the model to incorporate current and earlier fusion results rather than focusing solely on the current fusion step.

the VWAP of all filtered trades executed within the final trading hour before delivery, capturing the market’s last-minute imbalance needs. The distribution and seasonal patterns of the four indices can be seen in Figure 2. We formulate the intraday price index  $ID_x$  as:

$$ID_x = \frac{\sum_{s \in \{b, o\}} \sum_{t \in [t_1, t_2]} P_t^{(s)} V_t^{(s)}}{\sum_{s \in \{b, o\}} \sum_{t \in [t_1, t_2]} V_t^{(s)}}, \quad (1)$$

where  $s$  indicates the market side, with  $s \in \{b, o\}$  representing the bid (b) and offer (o) sides. Here,  $P_t^{(s)}$  and  $V_t^{(s)}$  denote the price and volume, respectively.  $t_1$  represents the prediction time (at which we predict future prices), while  $t_2$  denotes the delivery start time of electricity, introduced in Section 3.1.

Moreover, relationship between  $t_1$  and  $t_2$  is given by:

$$t_1 = t_2 - \Delta \quad (2)$$

where  $\Delta = 60 \times x$  min, with  $x = 1$  for  $ID_1$  and  $x = 3$  for  $ID_3$ .

## 4. OrderFusion Network

### 4.1. Encoding

The OrderFusion encoding method extracts features from the filtered orderbook and forms a 2.5D representation. In detail, given a prediction time  $t_1$  and a side  $s$ , we extract four features from a set of price and volume data  $\{P_t^{(s)}, V_t^{(s)}\}$  within the time interval  $[t_1 - \nabla, t_1]$ :

- Minimum price:  $p_{\min}^{(\nabla)}$
- Maximum price:  $p_{\max}^{(\nabla)}$
- VWAP:  $VWAP^{(\nabla)}$
- Total traded volume:  $v_{\text{sum}}^{(\nabla)}$

where  $\nabla$  represents look-back window length. Specifically, we consider six window lengths:

$$\nabla \in \{1 \text{ min}, 5 \text{ min}, 15 \text{ min}, 60 \text{ min}, 180 \text{ min}, \nabla_{\text{full}}\} \quad (3)$$

where  $\nabla_{\text{full}}$  denotes the complete history from market opening (15:00 on the previous day) to  $t_1$ .

This results in two separate feature maps (2.5D encoding)  $M^{(b)}, M^{(o)} \in \mathbb{R}^{d \times f}$  for bid and offer, respectively. Here,  $d = |\nabla| = 6$  represents the number of look-back window lengths, while  $f = 4$  corresponds to the number of extracted features per window, shown in Figure 1.

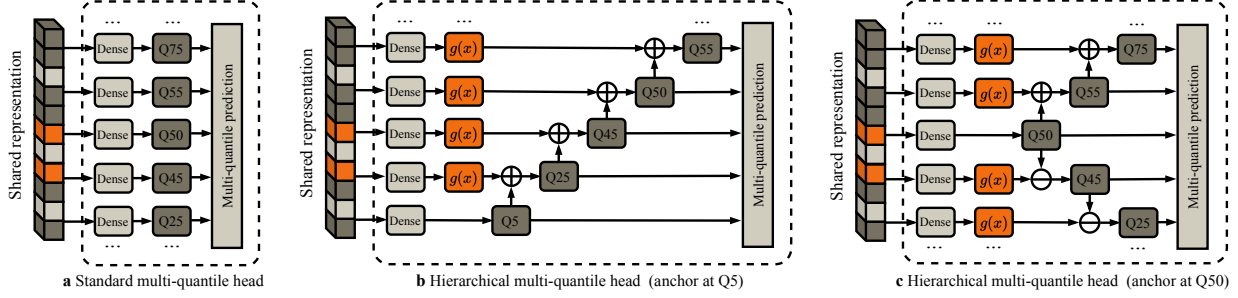


Figure 4. Comparison of different multi-quantile prediction architectures. **a**, Standard multi-quantile head. Each quantile is predicted using separate dense layers from a shared representation, leading to potential quantile crossing issues. **b**, Hierarchical multi-quantile head introduced in (Park et al., 2022): Anchored at the lowest quantile (Q5), and subsequent quantiles are computed hierarchically by adding a non-negative residual learned from a shared representation. This structure ensures monotonicity but may suffer from error accumulation. **c**, Hierarchical multi-quantile head (ours): Anchored at the median quantile (Q50), with both higher and lower quantiles computed hierarchically via non-negative residuals. This approach prevents quantile crossing while mitigating error accumulation.

## 4.2. Backbone

We introduce a tailored jump cross-attention backbone that takes the 2.5D encoding obtained via OrderFusion as input to model interdependencies between bids and offers. Specifically, the jump cross-attention backbone consists of several 1D-convolutional layers and cross-attention layers.

**1D-Convolution** We denote  $\mathbf{Z}_k^{(s)}$  as the input representation, where  $\mathbf{Z}_k^{(s)}$  can be either the bid representation ( $s = b$ ) or the offer representation ( $s = o$ ), and  $k$  represents the  $k$ th layer:

$$\mathbf{Z}_k^{(s)} = \begin{cases} \mathbf{M}^{(s)}, & \text{if } k = 0 \\ \mathbf{A}_k^{(s)}, & \text{otherwise} \end{cases} \quad (4)$$

where  $\mathbf{A}_k^{(s)}$  denotes the output from the cross-attention layer, which will be introduced shortly.

We employ a filter size of  $F$ , a kernel size of 1, a stride of 1, and no pooling. The transformation is expressed as:

$$\mathbf{C}_{k+1}^{(s)} = \text{Conv1D}(\mathbf{Z}_k^{(s)}) \quad (5)$$

where  $\mathbf{C}_{k+1}^{(s)} \in \mathbb{R}^{d \times F}$  is the transformed bid or offer feature representations through convolution.

**Cross-Attention** The cross-attention mechanism takes the bid and offer representations learned from 1D-conv layers as inputs. The first input (either bid or ask) is used to project the query, while the second input (another side) is utilized to project the key and value, respectively. When  $k$  is even, the second input is ‘‘jumped’’ to the  $k - 1$ th 1D-conv layer,

as illustrated in Figure 3. Precisely:

$$\mathbf{A}_k^{(s)} = \begin{cases} \text{CrossAttention}(\mathbf{C}_k^{(s)}, \mathbf{C}_{k-1}^{(\bar{s})}), & \text{if } k \text{ is even,} \\ \text{CrossAttention}(\mathbf{C}_k^{(s)}, \mathbf{C}_k^{(\bar{s})}), & \text{otherwise.} \end{cases} \quad (6)$$

where  $\bar{s}$  denotes the opposite side. For example, if  $s = b$ , then  $\bar{s} = o$ , and vice versa.

In detail, the CrossAttention operation is based on the multi-head attention (MHA) mechanism. Given input representations  $\mathbf{C}^{(s)} \in \mathbb{R}^{d \times F}$  and  $\mathbf{C}^{(\bar{s})} \in \mathbb{R}^{d \times F}$ , the query, key, and value matrices for each attention head are computed as:

$$\mathbf{Q}^{(s)}[h] = \mathbf{C}^{(s)} \mathbf{W}_Q^{(s)}[h], \quad (7)$$

$$\mathbf{K}^{(\bar{s})}[h] = \mathbf{C}^{(\bar{s})} \mathbf{W}_K^{(\bar{s})}[h], \quad (8)$$

$$\mathbf{V}^{(\bar{s})}[h] = \mathbf{C}^{(\bar{s})} \mathbf{W}_V^{(\bar{s})}[h] \quad (9)$$

where  $\mathbf{W}_Q^{(s)}[h], \mathbf{W}_K^{(\bar{s})}[h], \mathbf{W}_V^{(\bar{s})}[h] \in \mathbb{R}^{F \times d_h}$  are trainable projection matrices for the  $h$ -th attention head, and  $d_h = F/H$  is the head dimension for  $H$  attention heads. The scaled dot-product attention is applied:

$$\mathbf{A}^{(s)}[h] = \text{softmax} \left( \frac{\mathbf{Q}^{(s)}[h] \mathbf{K}^{(\bar{s})\top}[h]}{\sqrt{d_h}} \right) \mathbf{V}^{(\bar{s})}[h]. \quad (10)$$

The outputs of all attention heads are concatenated and linearly projected:

$$\mathbf{A}^{(s)} = (\mathbf{A}^{(s)}[1] \parallel \mathbf{A}^{(s)}[2] \parallel \dots \parallel \mathbf{A}^{(s)}[H]) \mathbf{W}^O, \quad (11)$$

where  $\mathbf{W}^O \in \mathbb{R}^{F \times F}$  is the projection matrix, and  $\parallel$  denotes concatenation.

The output  $\mathbf{A}^{(s)}$  has a special interpretation: it represents the augmented attention feature for side  $s$ , contextualized



by information from the opposite side  $\bar{s}$ . The formulation has intuition from game theory, where buyers adjust their bids based on information from the seller’s side, and vice versa. By incorporating cross-side dependencies, this mechanism allows the model to capture strategic interactions between bid and offer representations. Moreover, the equation introduced in (6) allows the model to not only extract interdependencies from the current layer but also focus on the previous layer, enabling deeper feature interactions.

The final feature vector  $\mathbf{U} \in \mathbb{R}^{2dF}$  is formed by concatenating flattened representations of outputs from jump cross-attention blocks, where  $2dF$  derives from two  $d \times F$  matrices.

### 4.3. Head

We design a hierarchical multi-quantile head that estimates a set of quantiles (Q5, Q25, Q45, Q50, Q55, Q75, Q95) hierarchically and overcomes the quantile crossing issue. The structure learns the median quantile ( $\tau = 0.5$ ) from the shared representation  $\mathbf{U} \in \mathbb{R}^{2dF}$  with one dense layer, shown in Figure 4. For quantiles above the median ( $\tau > 0.5$ ), the residuals are predicted using the same shared representation with other dense layers, denoted as  $r_{\tau'}$ , which are enforced to be non-negative using a non-negative function  $g(x)$ , e.g., ReLU. The upper quantile predictions ( $\hat{y}_{\tau'}$ ) are then computed iteratively by adding the non-negative residuals to the prediction of the preceding quantile ( $\tau$ ):

$$\hat{y}_{\tau'} = \hat{y}_{\tau} + g(r_{\tau'}), \quad (12)$$

where  $\tau$  is the nearest smaller quantile.

For quantiles below the median ( $\tau < 0.5$ ), the residuals  $r_{\tau'}$  are similarly enforced to be non-negative. The lower quantile predictions ( $\hat{y}_{\tau'}$ ) are computed iteratively by subtracting the non-negative residuals from the prediction of the preceding quantile ( $\tau$ ):

$$\hat{y}_{\tau'} = \hat{y}_{\tau} - g(r_{\tau'}), \quad (13)$$

where  $\tau$  is the nearest larger quantile.

### 4.4. Loss

Average quantile loss (AQL) is employed to estimate conditional quantiles of the target distribution. For a given quantile level  $\tau \in (0, 1)$ , the quantile loss  $L_{\tau}$  is defined as:

$$L_{\tau}(y_i, \hat{y}_{\tau,i}) = \begin{cases} \tau \cdot (y_i - \hat{y}_i), & \text{if } y_i \geq \hat{y}_i, \\ (1 - \tau) \cdot (\hat{y}_i - y_i), & \text{if } y_i < \hat{y}_i, \end{cases} \quad (14)$$

where  $y_i$  is the true value and  $\hat{y}_i$  is the predicted quantile for the  $i$ -th sample. This loss penalizes over-predictions and under-predictions differently depending on the quantile level  $\tau$ . When predicting upper quantiles ( $\tau > 0.5$ ), higher

penalties are applied to under-predictions, whereas for lower quantiles ( $\tau < 0.5$ ), over-predictions incur higher penalties.

Since our model employs a multi-task learning framework, the AQL is computed as the mean quantile loss across all samples and quantiles:

$$\text{AQL} = \frac{1}{|\mathcal{Q}|N} \sum_{\tau \in \mathcal{Q}} \sum_{i=1}^N L_{\tau}(y_i, \hat{y}_{\tau,i}), \quad (15)$$

where  $\mathcal{Q}$  represents the set of quantiles being predicted, and  $N$  is the total number of samples. Lower AQL values indicate better overall performance in quantile prediction.

## 4.5. Other Details

We use the Adam optimizer (Kingma & Ba, 2015), with an initial learning rate of  $3 \times 10^{-4}$ , which decays exponentially at a rate of 0.7 every 10 epochs. The number of training epochs is set to 50, from which we select the best model with the lowest validation loss. The batch size is configured as 2048 to maximize the usage efficiency of A100 GPU. The activation function employed in the backbone is Swish (Ramachandran et al., 2017).

## 5. Experiments

### 5.1. Data Splitting

The orderbook data are split into training, validation, and testing. The training period spans from January 2022 to December 2023, the validation period covers January 2024 to June 2024, and the testing period is set from July 2024 to December 2024.

### 5.2. Rolling-Window Approach

Predictions are made with a rolling window approach tailored to the granularity of the target price indices. For 15-minute price indices (15-min ID<sub>3</sub> and 15-min ID<sub>1</sub>), predictions are generated every 15 minutes. For 60-minute price indices (60-min ID<sub>3</sub> and 60-min ID<sub>1</sub>), predictions are generated on an hourly basis. If the prediction target is ID<sub>3</sub>, the prediction is made 3 hours in advance, while for ID<sub>1</sub>, predictions are made 1 hour before the delivery time.

### 5.3. Benchmarks

**Encoding Methods** We compare 1D, 2D, 3D, and our proposed 2.5D encoding method (OrderFusion) with different backbones. The 1D encoding flattens feature representations and applies a Multi-Layer Perceptron (MLP) as the backbone. The 2D encoding adopts a time-series format, where Long Short-Term Memory (LSTM) and Gated Recurrent Unit (GRU) layers process sequential data. The 3D encoding converts the data into a 3D pseudo-image representation

Table 1. Performance metrics for different methods and configurations (mean±std) on four price indices (60-min ID<sub>3</sub>, 60-min ID<sub>1</sub>, 15-min ID<sub>3</sub>, and 15-min ID<sub>1</sub>) with 5 runs. Five methods (MLP, LSMT, GRU, CNN, and ours) are compared. The best results are shown in **bold**, and the second-best results are underlined. Metrics include AQL and AQCR for probabilistic evaluation across all quantiles, and RMSE, MAE, and R<sup>2</sup> for pointwise evaluation of the median quantile. The total number of parameters of each model is identically constrained to 10<sup>5</sup> for a fair comparison.

PRICE INDEX	MODEL	AQL ↓	AQCR ↓	RMSE ↓	MAE ↓	R <sup>2</sup> ↑
60-MIN ID <sub>3</sub>	MLP	5.01±0.07	36.62±0.92	40.13±0.60	12.61±0.24	0.77±0.01
	LSTM	5.20±0.18	15.40±16.24	41.20±1.40	13.11±0.42	0.76±0.02
	GRU	4.96±0.06	<u>12.48±4.20</u>	<u>39.86±0.09</u>	<u>12.47±0.14</u>	<u>0.77±0.00</u>
	CNN	4.81±0.04	16.60±2.31	39.89±0.40	11.99±0.15	0.77±0.00
	OURS	<b>4.68±0.03</b>	<b>0.00±0.00</b>	<b>39.30±0.13</b>	<b>11.81±0.06</b>	<b>0.78±0.00</b>
60-MIN ID <sub>1</sub>	MLP	5.66±0.09	40.50±2.53	59.53±0.77	14.22±0.16	0.68±0.01
	LSTM	6.07±0.14	<u>11.60±6.03</u>	62.69±3.24	15.00±0.38	0.64±0.04
	GRU	5.77±0.05	13.60±7.39	61.33±1.13	14.47±0.11	0.66±0.01
	CNN	5.41±0.06	26.27±4.32	<u>59.51±0.41</u>	<u>13.67±0.14</u>	<u>0.68±0.00</u>
	OURS	<b>5.37±0.04</b>	<b>0.00±0.00</b>	<b>59.02±0.77</b>	<b>13.50±0.06</b>	<b>0.68±0.01</b>
15-MIN ID <sub>3</sub>	MLP	22.17±2.02	78.97±4.97	97.56±10.93	53.81±12.20	0.16±0.18
	LSTM	17.91±3.24	<u>38.41±20.38</u>	90.71±7.45	43.35±4.58	0.28±0.12
	GRU	<u>16.28±3.96</u>	49.14±26.72	<u>84.17±6.49</u>	<u>41.15±9.34</u>	<u>0.38±0.09</u>
	CNN	16.51±2.78	77.36±1.28	89.46±12.76	46.53±17.22	0.29±0.21
	OURS	<b>8.11±0.04</b>	<b>0.00±0.00</b>	<b>71.73±1.07</b>	<b>20.33±0.10</b>	<b>0.55±0.01</b>
15-MIN ID <sub>1</sub>	MLP	26.94±1.37	88.37±8.47	116.14±10.48	63.51±13.63	0.20±0.14
	LSTM	18.81±1.30	<u>63.10±6.06</u>	<u>96.22±1.80</u>	<u>40.96±3.56</u>	<u>0.45±0.02</u>
	GRU	20.07±3.13	72.24±4.43	102.12±9.13	46.52±4.93	0.38±0.11
	CNN	20.60±1.41	86.05±5.59	102.59±5.40	48.36±6.53	0.38±0.06
	OURS	<b>12.93±4.49</b>	<b>0.00±0.00</b>	<b>88.73±6.79</b>	<b>32.12±11.16</b>	<b>0.53±0.07</b>

and utilizes a 2D convolutional backbone. The proposed OrderFusion method transforms the orderbook into a 2.5D encoding and a tailored jump cross-attention backbone is used.

For a fair comparison, hyperparameters such as optimizer, learning rate, training epochs, batch size, and activation function are set the same for all benchmarks, as described in Section 4.5. Furthermore, the total number of parameters for each model is controlled to remain identical. Additional details of the benchmarks are provided in Appendix A.1.

#### 5.4. Evaluation Metrics

**Probabilistic Prediction** We evaluate the testing performance of probabilistic prediction using AQL, described in Section 4.4, and the average quantile crossing rate (AQCR), shown below:

AQCR is utilized to quantify the frequency of quantile crossing violations. The quantile crossing indicator for a quantile pair  $(\tau_l, \tau_u)$  with  $\tau_l < \tau_u$  is:

$$C_{\tau_l, \tau_u}(\hat{y}_{l,i}, \hat{y}_{u,i}) = \mathbb{I}(\hat{y}_{l,i} > \hat{y}_{u,i}), \quad (16)$$

where  $\mathbb{I}(\cdot)$  is an indicator function that returns 1 if the condition inside is true and 0 otherwise.

We aggregate the crossing indicators to compute the AQCR

across  $N$  samples as:

$$\text{AQCR} = \frac{1}{N} \sum_{i=1}^N C_{\tau_l, \tau_u}(\hat{y}_{l,i}, \hat{y}_{u,i}), \quad (17)$$

Smaller AQCR values indicate fewer quantile crossing violations, reflecting more reliable quantile predictions.

**Pointwise Prediction** We use the root mean squared error (RMSE), mean absolute error (MAE), and R<sup>2</sup> as evaluation metrics for the pointwise prediction of the median quantile. The details can be found in Appendix A.2.

#### 5.5. Results

The results presented in Table 1 demonstrate the experimental performance of our proposed methods compared to the benchmarks. Generally, the prediction losses for ID<sub>1</sub> are higher than those for ID<sub>3</sub>, as ID<sub>1</sub> represents the last-minute imbalance needs, making it more volatile. Furthermore, losses for 15-minute price indices are notably higher than those for 60-minute indices, highlighting the increased volatility of 15-minute prices.

**Parameter Efficiency** Figure 5 illustrates the parameter scaling law of five models. With the same number of param-

Table 2. Ablation studies for three backbones (No cross-attention, Standard cross-attention, Jump cross-attention)

PRICE INDEX	CROSS-ATTENTION	AQL ↓	AQCR ↓	RMSE ↓	MAE ↓	R <sup>2</sup> ↑
60-MIN ID <sub>3</sub>	NONE	4.73±0.11	<b>0.00±0.00</b>	39.40±0.10	11.92±0.14	0.78±0.00
	STANDARD	4.77±0.04	<b>0.00±0.00</b>	39.84±0.20	11.99±0.08	0.77±0.00
	JUMP	<b>4.68±0.03</b>	<b>0.00±0.00</b>	<b>39.30±0.13</b>	<b>11.81±0.06</b>	<b>0.78±0.00</b>
60-MIN ID <sub>1</sub>	NONE	<b>5.34±0.10</b>	<b>0.00±0.00</b>	60.72±0.78	13.51±0.15	0.67±0.01
	STANDARD	5.53±0.02	<b>0.00±0.00</b>	60.36±0.74	13.86±0.06	0.67±0.01
	JUMP	5.37±0.04	<b>0.00±0.00</b>	<b>59.02±0.77</b>	<b>13.50±0.06</b>	<b>0.68±0.01</b>
15-MIN ID <sub>3</sub>	NONE	12.41±1.59	<b>0.00±0.00</b>	75.43±0.55	27.11±1.57	0.51±0.01
	STANDARD	9.06±0.62	<b>0.00±0.00</b>	73.76±0.83	22.92±1.88	0.53±0.01
	JUMP	<b>8.11±0.04</b>	<b>0.00±0.00</b>	<b>71.73±1.07</b>	<b>20.33±0.10</b>	<b>0.55±0.01</b>
15-MIN ID <sub>1</sub>	NONE	15.85±3.25	<b>0.00±0.00</b>	90.20±4.31	36.55±8.32	0.52±0.05
	STANDARD	13.51±0.84	<b>0.00±0.00</b>	<b>87.92±2.18</b>	<b>31.23±3.24</b>	<b>0.54±0.02</b>
	JUMP	<b>12.93±4.49</b>	<b>0.00±0.00</b>	88.73±6.79	32.12±11.16	0.53±0.07

Table 3. Ablation studies for three heads (Standard, Hierarchical anchored at Q5, and Hierarchical anchored at Q50)

PRICE INDEX	MODEL	AQL ↓	AQCR ↓	RMSE ↓	MAE ↓	R <sup>2</sup> ↑
60-MIN ID <sub>3</sub>	STANDARD	4.70±0.04	2.12±2.84	<b>39.20±0.10</b>	11.85±0.09	<b>0.78±0.00</b>
	HIER. Q5	4.74±0.06	<b>0.00±0.00</b>	39.27±0.16	11.89±0.09	0.78±0.00
	HIER. Q50	<b>4.68±0.03</b>	<b>0.00±0.00</b>	39.30±0.13	<b>11.81±0.06</b>	<b>0.78±0.00</b>
60-MIN ID <sub>1</sub>	STANDARD	<b>5.32±0.03</b>	3.81±2.24	<b>57.74±0.44</b>	<b>13.44±0.08</b>	<b>0.70±0.01</b>
	HIER. Q5	5.41±0.11	<b>0.00±0.00</b>	58.45±0.76	13.53±0.20	0.69±0.01
	HIER. Q50	5.37±0.04	<b>0.00±0.00</b>	59.02±0.77	13.50±0.06	0.68±0.01
15-MIN ID <sub>3</sub>	STANDARD	8.19±0.12	3.61±6.75	<b>71.07±1.35</b>	20.48±0.28	<b>0.56±0.02</b>
	HIER. Q5	8.18±0.05	<b>0.00±0.00</b>	71.82±0.70	20.43±0.13	0.55±0.01
	HIER. Q50	<b>8.11±0.04</b>	<b>0.00±0.00</b>	71.73±1.07	<b>20.33±0.10</b>	0.55±0.01
15-MIN ID <sub>1</sub>	STANDARD	<b>12.36±2.01</b>	22.77±17.33	<b>86.37±4.51</b>	<b>29.33±3.90</b>	<b>0.56±0.05</b>
	HIER. Q5	15.89±7.17	<b>0.00±0.00</b>	93.86±19.28	39.90±20.92	0.46±0.24
	HIER. Q50	12.93±4.49	<b>0.00±0.00</b>	88.73±6.79	32.12±11.16	0.53±0.07

eters ( $10^4$ ,  $10^5$ ,  $10^6$ ), our approach consistently achieves superior performance. Furthermore, increasing the parameter count from  $10^5$  to  $10^6$  results in only marginal improvements, indicating that our model requires fewer parameters to reach performance saturation. Table 1 provides a detailed comparison across various metrics, with all models constrained to  $10^5$  parameters. The best results are consistently achieved with our proposed method. Especially, our method surpasses GRU by 50.3% for 15min-ID<sub>3</sub> and LSTM by 31.3% for 15min-ID<sub>1</sub> in AQL. These results indicate that LSTM and GRU suffer from underfitting and require more parameters to achieve proper performance, and our model is particularly parameter-efficient for volatile 15-min indices.

**Reliability** Observed from Table 1, the AQCR of our proposed method is consistently zero, indicating no quantile crossing. This result is expected, as our design strictly enforces monotonicity between quantiles. In contrast, the 1D encoding with MLP performs the worst, with an average

AQCR of 61.1% across four indices, leading to unreliable forecasts. The high AQCR from MLP further highlights the importance of proper data encoding.

### 5.6. Ablation Studies

**Cross-Attention** We implement and compare three backbone architectures: (1) a backbone without cross-attention, (2) a standard cross-attention backbone, and (3) our proposed jump cross-attention backbone. Three models employ the same hierarchical head anchored at Q50, with  $10^5$  parameters. A comparison of these architectures is shown in Figure 3. Observed from Table 2, our tailored jump cross-attention outperforms the other two backbones across most metrics. Additionally, compared to the baseline model without cross-attention, the results highlight that introducing cross-attention improves 20.85% AQL on average in forecasting volatile 15-min prices.



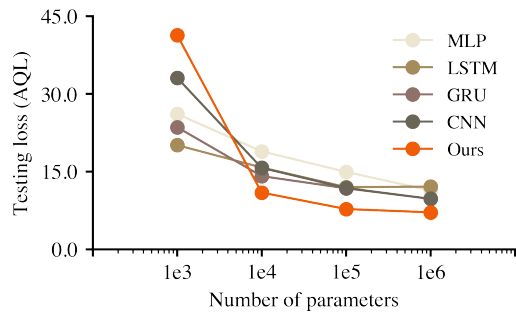


Figure 5. Model comparison with a different number of parameters. The x-axis represents the number of parameters (on a logarithmic scale), while the y-axis shows the mean testing AQL aggregated across all price indices.

**Multi-Quantile Head** We implement and compare three multi-quantile heads: (1) a standard multi-quantile head, (2) a hierarchical multi-quantile head anchored at Q5 (Park et al., 2022), and (3) our proposed hierarchical multi-quantile head anchored at Q50. A comparison of these architectures is illustrated in Figure 4. Three heads incorporate OrderFusion and jump cross-attention with  $10^5$  parameters. Notably, removing the monotonic constraint improves certain metrics, consistent with observations from (Park et al., 2022). However, our model still outperforms other benchmarks across all metrics. Compared to the hierarchical head anchored at Q5, our approach achieves 18.6% lower AQL and 19.5% lower MAE for 15min-ID1 as our method reduces the risk of error accumulation.

## 6. Conclusion

In conclusion, our proposed OrderFusion framework, combined with a jump cross-attention backbone, enables parameter-efficient learning, highlighting the importance of modeling interdependencies between bids and offers through variants of cross-attention. The designed hierarchical multi-quantile head anchored at Q50 predicts multiple quantiles simultaneously while addressing the quantile crossing issue and mitigating the risk of error accumulation for volatile price indices. Experimental results and ablation studies demonstrate the efficiency and reliability of our approach. This work lays the foundation for future advancements in probabilistic modeling within the energy domain, particularly for high-frequency, volatile CID markets.

## Impact Statement

Our proposed encoding method is applicable to all European CID markets, as the orderbook data from EPEX

Spot follows a uniform structure. The designed hierarchical multi-quantile head can be seamlessly integrated with various backbones for diverse probabilistic prediction tasks while overcoming quantile crossing issues. By providing a parameter-efficient and reliable prediction framework, our model contributes to enhanced uncertainty management and supports a smoother transition toward renewable energy integration.

**Data availability** Data cannot be shared due to commercial restrictions.

**Code availability** Codes will be made publicly available.

## References

- Afham, M., Dissanayake, I., Dissanayake, D., Dharmasiri, A., Thilakarathna, K., and Rodrigo, R. Crosspoint: Self-supervised cross-modal contrastive learning for 3d point cloud understanding. In *Proceedings of the IEEE/CVF Conference on Computer Vision and Pattern Recognition*, pp. 9902–9912, 2022.
- Andrade, J. R., Filipe, J., Reis, M., and Bessa, R. J. Probabilistic price forecasting for day-ahead and intraday markets: Beyond the statistical model. *Sustainability*, 9(11): 1990, 2017.
- Chen, C.-F. R., Fan, Q., and Panda, R. Crossvit: Cross-attention multi-scale vision transformer for image classification. In *Proceedings of the IEEE/CVF international conference on computer vision*, pp. 357–366, 2021.
- Chernozhukov, V., Fernández-Val, I., and Galichon, A. Quantile and probability curves without crossing. *Econometrica*, 78(3):1093–1125, 2010. doi: <https://doi.org/10.3982/ECTA7880>. URL <https://onlinelibrary.wiley.com/doi/abs/10.3982/ECTA7880>.
- Cho, K., Van Merriënboer, B., Gulcehre, C., Bahdanau, D., Bougares, F., Schwenk, H., and Bengio, Y. Learning phrase representations using rnn encoder-decoder for statistical machine translation. *arXiv preprint arXiv:1406.1078*, 2014.
- Cramer, E., Witthaut, D., Mitsos, A., and Dahmen, M. Multivariate probabilistic forecasting of intraday electricity prices using normalizing flows. *Applied Energy*, 346: 121370, 2023.
- Fei, B., Yang, W., Ma, L., and Chen, W.-M. Dctr: Noise-robust point cloud completion by dual-channel transformer with cross-attention. *Pattern Recognition*, 133: 109051, 2023.

- Hirsch, S. and Ziel, F. Multivariate simulation-based forecasting for intraday power markets: Modeling cross-product price effects. *Applied Stochastic Models in Business and Industry*, 2024a.
- Hirsch, S. and Ziel, F. Simulation-based forecasting for intraday power markets: Modelling fundamental drivers for location, shape and scale of the price distribution. *The Energy Journal*, 45(3):107–144, 2024b.
- Hochreiter, S. Long short-term memory. *Neural Computation MIT-Press*, 1997.
- Janke, T. and Steinke, F. Forecasting the price distribution of continuous intraday electricity trading. *Energies*, 12(22):4262, 2019.
- Jawed, S. and Schmidt-Thieme, L. Gqformer: A multi-quantile generative transformer for time series forecasting. In *2022 IEEE International Conference on Big Data (Big Data)*, pp. 992–1001. IEEE, 2022.
- Kingma, D. and Ba, J. Adam: A method for stochastic optimization. In *International Conference on Learning Representations (ICLR)*, San Diego, CA, USA, 2015.
- Koch, C. and Hirth, L. Short-term electricity trading for system balancing: An empirical analysis of the role of intraday trading in balancing germany’s electricity system. *Renewable and Sustainable Energy Reviews*, 113:109275, 2019.
- LeCun, Y., Bottou, L., Bengio, Y., and Haffner, P. Gradient-based learning applied to document recognition. *Proceedings of the IEEE*, 86(11):2278–2324, 1998.
- Lim, B., Arık, S. Ö., Loeff, N., and Pfister, T. Temporal fusion transformers for interpretable multi-horizon time series forecasting. *International Journal of Forecasting*, 37(4):1748–1764, 2021.
- Maciejowska, K. and Nowotarski, J. A hybrid model for gefcom2014 probabilistic electricity price forecasting. *International Journal of Forecasting*, 32(3):1051–1056, 2016. ISSN 0169-2070. doi: <https://doi.org/10.1016/j.ijforecast.2015.11.008>.
- Marcjasz, G., Uniejewski, B., and Weron, R. Beating the naïve—combining lasso with naïve intraday electricity price forecasts. *Energies*, 13(7), 2020. ISSN 1996-1073. doi: [10.3390/en13071667](https://doi.org/10.3390/en13071667).
- Monteiro, C., Ramirez-Rosado, I. J., Fernandez-Jimenez, L. A., and Conde, P. Short-term price forecasting models based on artificial neural networks for intraday sessions in the iberian electricity market. *Energies*, 9(9):721, 2016.
- Narajewski, M. and Ziel, F. Econometric modelling and forecasting of intraday electricity prices. *Journal of Commodity Markets*, 19:100107, 2020a.
- Narajewski, M. and Ziel, F. Ensemble forecasting for intraday electricity prices: Simulating trajectories. *Applied Energy*, 279:115801, 2020b.
- Ocker, F. and Ehrhart, K.-M. The “german paradox” in the balancing power markets. *Renewable and Sustainable Energy Reviews*, 67:892–898, 2017. ISSN 1364-0321. doi: <https://doi.org/10.1016/j.rser.2016.09.040>.
- Oksuz, I. and Ugurlu, U. Neural network based model comparison for intraday electricity price forecasting. *Energies*, 12(23):4557, 2019.
- Park, Y., Maddix, D., Aubet, F.-X., Kan, K., Gasthaus, J., and Wang, Y. Learning quantile functions without quantile crossing for distribution-free time series forecasting. In Camps-Valls, G., Ruiz, F. J. R., and Valera, I. (eds.), *Proceedings of The 25th International Conference on Artificial Intelligence and Statistics*, volume 151 of *Proceedings of Machine Learning Research*, pp. 8127–8150. PMLR, 28–30 Mar 2022.
- Ramachandran, P., Zoph, B., and Le, Q. V. Searching for activation functions. *arXiv preprint arXiv:1710.05941*, 2017.
- Rodrigues, F. and Pereira, F. C. Beyond expectation: Deep joint mean and quantile regression for spatiotemporal problems. *IEEE transactions on neural networks and learning systems*, 31(12):5377–5389, 2020.
- Rumelhart, D. E., Hinton, G. E., and Williams, R. J. Learning representations by back-propagating errors. *nature*, 323(6088):533–536, 1986.
- Serafin, T., Uniejewski, B., and Weron, R. Averaging predictive distributions across calibration windows for day-ahead electricity price forecasting. *Energies*, 12(13), 2019. ISSN 1996-1073. doi: [10.3390/en12132561](https://doi.org/10.3390/en12132561).
- Serafin, T., Marcjasz, G., and Weron, R. Trading on short-term path forecasts of intraday electricity prices. *Energy Economics*, 112:106125, 2022.
- Uniejewski, B., Marcjasz, G., and Weron, R. Understanding intraday electricity markets: Variable selection and very short-term price forecasting using lasso. *International Journal of Forecasting*, 35(4):1533–1547, 2019. ISSN 0169-2070. doi: <https://doi.org/10.1016/j.ijforecast.2019.02.001>.
- Zhang, Y. and Yan, J. Crossformer: Transformer utilizing cross-dimension dependency for multivariate time series forecasting. In *The eleventh international conference on learning representations*, 2023.

---

**Algorithm 2** Matching Rule

---

**Input:** Bids  $(P^{(b)}, V^{(b)})$ , Offers  $(P^{(o)}, V^{(o)})$   
**if**  $P^{(b)} \geq P^{(o)}$  **then**  
    **if**  $V^{(b)} = V^{(o)}$  **then**  
        **Full execution:** Match full volumes and remove both orders from the orderbook.  
    **else**  
        **Partial execution:** Match partial volumes and update the remaining order.  
    **end if**  
**else**  
    **No execution:** Leave both orders in the orderbook.  
**end if**

---

## A. Appendix

### A.1. Benchmark Models

**MLP** Multilayer Perceptrons (MLPs) (Rumelhart et al., 1986) are effective for tabular data and simple classification or regression tasks, learning nonlinear relationships through fully connected layers. While they excel in static pattern recognition, they struggle with sequential dependencies and require regularization to prevent overfitting. In our setup, we use 4 dense layers and adjust the number of neurons to match the total parameter count of other models, keeping the remaining hyperparameters identical to those in Section 4.5.

**LSTM** Long Short-Term Memory (LSTM) networks (Hochreiter, 1997) are well-suited for sequential data, capturing long-term dependencies through memory cells and gating mechanisms. They mitigate vanishing gradients but have high computational costs. In our experiments, we use 4 LSTM layers, adjusting the number of hidden units to control the total parameter count, with other hyperparameters kept consistent as described in Section 4.5.

**GRU** Gated Recurrent Units (GRUs) (Cho et al., 2014) offer a more computationally efficient alternative to LSTMs by simplifying the gating mechanism. They balance short- and long-term dependencies but may underperform in highly complex sequences. Our implementation includes 4 GRU layers, tuning the number of units to control the total parameter count while maintaining consistent hyperparameter settings from Section 4.5.

**CNN** Convolutional Neural Networks (CNNs) (LeCun et al., 1998) are designed for spatial and temporal pattern extraction using learnable kernels. While 2D CNNs dominate image processing, 1D CNNs efficiently capture local temporal dependencies in time series. However, they lack inherent long-term sequence modeling. We employ 4 CNN layers, adjusting the number of filters to match the total parameter count, with other hyperparameters aligned with those in Section 4.5.

### A.2. Pointwise Metrics

**RMSE** The Root Mean Squared Error (RMSE) evaluates the accuracy of pointwise predictions by penalizing larger errors more heavily than smaller ones. It is particularly sensitive to outliers and provides an overall measure of prediction quality. RMSE is calculated as:

$$\text{RMSE} = \sqrt{\frac{1}{N} \sum_{i=1}^N (y_i - \hat{y}_i)^2}, \quad (18)$$

where  $y_i$  represents the true value,  $\hat{y}_i$  is the predicted value, and  $N$  is the total number of samples.

**MAE** The Mean Absolute Error (MAE) measures the average magnitude of prediction errors, treating all deviations equally regardless of their direction. Unlike RMSE, MAE is more robust to outliers, making it a reliable metric for assessing average prediction accuracy. It is computed as:

$$\text{MAE} = \frac{1}{N} \sum_{i=1}^N |y_i - \hat{y}_i|, \quad (19)$$

where  $y_i$  and  $\hat{y}_i$  are the true and predicted values, respectively.

$R^2$  The Coefficient of Determination ( $R^2$ ) quantifies the proportion of variance in the target variable that is explained by the predictions. A value of  $R^2 = 1$  indicates perfect predictions, whereas  $R^2 = 0$  suggests that the model performs no better than predicting the mean of the true values. It is defined as:

$$R^2 = 1 - \frac{\sum_{i=1}^N (y_i - \hat{y}_i)^2}{\sum_{i=1}^N (y_i - \bar{y})^2}, \quad (20)$$

where  $\bar{y}$  is the mean of the true values  $y_i$ , and the numerator and denominator represent the residual sum of squares and the total sum of squares, respectively.